# The Effect of Intracrystalline Water on the Mechanical Properties of Olivine at Room Temperature

**Kathryn M. Kumamoto[1,2,*], Lars N. Hansen[2], Thomas Breithaupt[3], David Wallis[3], Bo-Shiuan Li[4], David E.J. Armstrong[4], David L. Goldsby[5], Yang (Will) Li[2], Jessica M. Warren[6], and Angus J. Wilkinson[4]**

[1] Lawrence Livermore National Laboratory, Livermore, CA, USA

[2] Department of Earth and Environmental Sciences, University of Minnesota, Minneapolis, MN, USA

[3] Department of Earth Sciences, University of Cambridge, Cambridge, UK

[4] Department of Materials, University of Oxford, Oxford, UK

[5] Department of Earth and Environmental Science, University of Pennsylvania, PA, USA

[6] Department of Earth Sciences, University of Delaware, Newark, DE, USA

[*]corresponding author, kumamoto3@llnl.gov

## KEY POINTS

- Room-temperature nanoindentation tests on wet and dry olivine yield very similar mechanical results.
- Any effect of water incorporation on yield stress is outweighed by the effect of orientation anisotropy.
- Water may only weaken olivine at high temperatures and therefore not influence strength in the coldest portions of the lithosphere.

## ABSTRACT

The effect of small concentrations of intracrystalline water on the strength of olivine is significant at asthenospheric temperatures but is poorly constrained at lower temperatures applicable to the shallow lithosphere. We examined the effect of water on the yield stress of olivine during low-temperature plasticity using room-temperature Berkovich nanoindentation. The presence of water in olivine (1600 ppm H/Si) does not affect hardness or yield stress relative to dry olivine (≤40 ppm H/Si) outside of uncertainty but may slightly reduce Young's modulus. Differences between water-bearing and dry crystals in similar orientations were minor compared to differences between dry crystals in different orientations. These observations suggest water content does not affect the strength of olivine at low homologous temperatures. Thus, intracrystalline water does not play a role in olivine deformation at these temperatures, implying that water does not lead to weakening in the coldest portions of the mantle.



## PLAIN LANGUAGE SUMMARY

At high temperatures (>1000°C), incorporating small amounts of water in a crystalline structure can dramatically affect the strength of that crystal. There are many theories as to why this is the case, and each theory makes a prediction for how water might affect the strength of crystals at low temperatures. Thus, by conducting experiments at room temperature, we can distinguish between some of these theories. Our data indicate that water does not have a significant effect on the strength of olivine at room temperature, and any minor effect that water may have is far outweighed by the effect of crystal orientation. These observations rule out theories in which water causes a decrease in the strength of olivine at all temperatures, implying that water does not lead to weakening in the coldest portions of the mantle.

## 1. Introduction

The rheological behavior of the upper mantle is predominantly controlled by the mechanical response of olivine, its most common constituent mineral. The rate of deformation of olivine by the motion of dislocations can be limited by either dislocation glide or dislocation climb. Climb is the rate-controlling process at high temperatures and low stresses, commonly associated with the asthenosphere and lower lithosphere, while dislocation glide is rate-limiting at the low temperatures and high stresses typical of the shallow lithospheric mantle (c.f., Warren & Hansen, 2023). We refer to glide-controlled deformation as low-temperature plasticity (LTP). Glide velocity is predominantly controlled by the Peierls stress, which is the resistance of the crystal lattice to dislocation glide in the absence of thermal activation (e.g., Karato, 2008, Chapter 9). Therefore, lattice resistance and the microphysical processes by which dislocations overcome it are important to determine over the full range of environmental and compositional variables at play in the upper mantle.

Olivine is a nominally anhydrous mineral in that it contains no stoichiometric water (e.g. Bell and Rossman, 1992). However, small concentrations of water (<0.01 wt% $H_2O$) can be hosted in the crystal structure of olivine in the form of $H^+$ ions, and these small concentrations can have dramatic effects on the physical properties of olivine, including viscosity (e.g., Kohlstedt, 2006) and electrical conductivity (Wang et al., 2006). As LTP typically occurs at relatively shallow depths where interaction between peridotites and hydrous fluids may be most common, constraining the impact of hydrous point defects on the rheological properties of olivine is important for understanding the deformation processes that occur in such settings. Examples include the plastic deformation of asperities on frictional faults (e.g., Boettcher et al., 2007) and the bending of plates entering subduction zones (e.g., Buffett & Becker, 2012).

To refine analyses of these deformation processes, we must distinguish among models that predict the impact of intracrystalline $H^+$ on LTP of olivine. There are several potential mechanisms by which small concentrations of $H^+$ may decrease the strength of nominally anhydrous minerals (e.g., Griggs, 1967; Hobbs, 1984; Katayama & Karato, 2008), and the role of water in glide-controlled deformation is still unclear. The presence of $H^+$ ions may modify the dynamics of dislocation glide through several aspects of the dislocation motion. Dislocation glide is generally considered to occur by the process of nucleation and migration of kinks, which

are local displacements of the dislocation line in its glide plane. As detailed in the supplemental material, flow laws based on the glide of dislocations can be derived to explicitly include the behavior of dislocation kinks. Several of the parameters in these flow laws may be affected by the concentration of $H^+$ (e.g., Hobbs, 1984). For instance, increasing the concentration of $H^+$ may lead to weakening by increasing the concentration of kinks. Weakening may also occur by decreasing the Peierls stress, the intrinsic resistance of the lattice to dislocation motion, or by decreasing the backstress, the resistance to dislocation motion by elastic interaction with other dislocations.

We group models for the role of water in LTP based on which of the flow-law parameters is primarily influenced by $H^+$ (Figure 1). We define models 1 and 2 as cases in which $H^+$ does not affect LTP, as suggested by Tielke et al. (2017). In model 1, the influence of water on deformation occurs only at high temperatures through its influence on the bulk diffusivities of the major species and therefore on dislocation climb and recovery (c.f., Kohlstedt, 2006), which reduces the backstress, and therefore, the steady-state flow stress (e.g., Breithaupt et al., 2023). In model 2, $H^+$ results in charged point defects that couple to the kink concentration through point-defect equilibria because kinks in ionic solids can be charged (Hobbs, 1984). As highlighted in the supplemental material, increasing the kink concentration has little effect during LTP and primarily reduces the flow stress during high-temperature creep. Other models consider $H^+$ to hydrolyze Si-O bonds (e.g., Griggs, 1967, 1974), which reduces the Peierls stress, as demonstrated for quartz by Heggie and Jones (1986). In model 3, as suggested by Griggs (1967, 1974), $H^+$ must continually diffuse along dislocation cores to reduce the Peierls stress in the vicinity of dislocations, which will only be effective above an apparent threshold temperature. In model 4 (Karato, 2008, equation 9.10; Katayama and Karato, 2008), this process is never limited by diffusion, and the weakening associated with a reduction in the Peierls stress occurs at all temperatures.

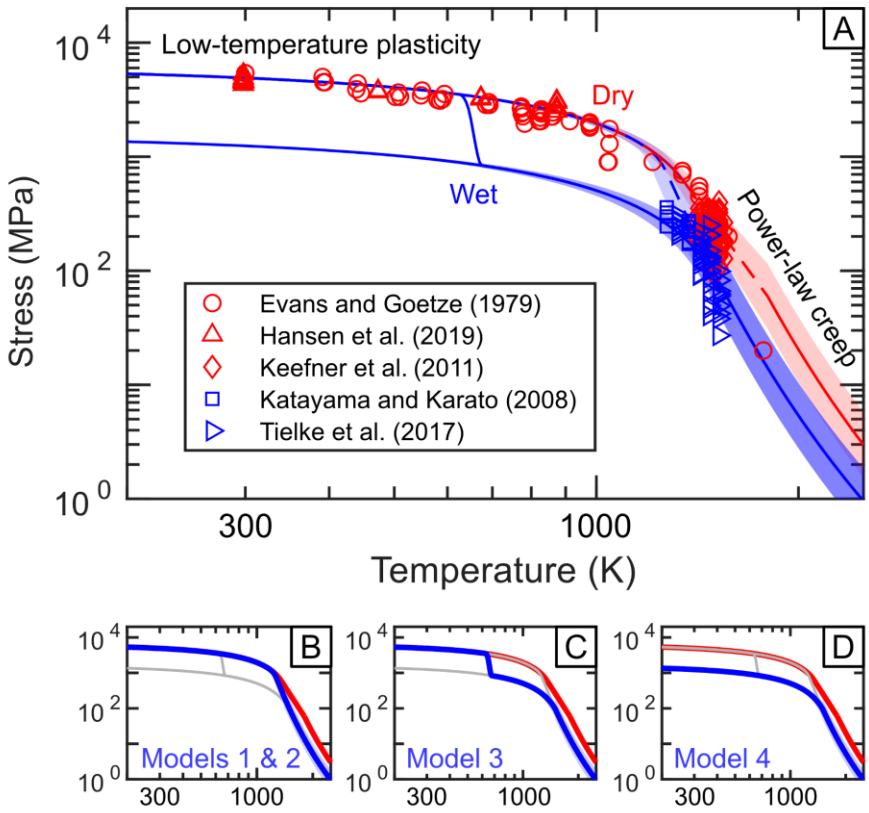


**Figure 1:** Stress as a function of temperature measured in experiments and predicted by models of hydrolytic weakening. (A) Models and data are shown in red for dry olivine (Evans & Goetze, 1979; Keefner et al., 2011; Hansen et al., 2019) and blue for wet olivine (Katayama & Karato, 2008; Tielke et al., 2017). Experimental data cover strain rates from $4.2 \times 10^{-7}$ to $4.4 \times 10^{-4}$ $s^{-1}$ and are plotted without normalization. Flow laws and models of hydrolytic weakening are shown as solid lines for a strain rate of $10^{-5}$ $s^{-1}$ with the minima and maxima of the shaded regions respectively indicating strain rates of $10^{-6}$ $s^{-1}$ and $10^{-4}$ $s^{-1}$. Dashed lines are schematic transitions between LTP and dislocation creep. Flow laws for power-law creep of wet and dry olivine are from Hirth and Kohlstedt (2003). The LTP flow law for dry olivine is from Hansen et al. (2021). Models 1, 2, and 3 of hydrolytic weakening in the low-temperature regime are schematic and are described in the text. Model 4 is based on the flow law of Katayama and Karato (2008). (B, C, D) Individual models of hydrolytic weakening are highlighted in blue, with dry LTP and dislocation creep in red. The axes of each panel are the same as in (A). See supplemental information for further details of plotted flow laws and models.

In this study, we aim to distinguish among these models by examining the yield strength of hydrated olivine compared to dry olivine using room-temperature nanoindentation. This technique, in which a small, hard stylus is pressed into a sample to leave a plastically-deformed impression, is commonly used to probe elasticity and plasticity in metals and industrial ceramics (e.g., Oliver & Pharr, 1992, 2004; Kalidindi & Vachhani, 2014). Recently, indentation methods have seen a rise in popularity in the geosciences due to their comparative ease of use, rapid data

acquisition, and reproducibility (e.g., Kranjc et al., 2016; Kumamoto et al., 2017; Thom & Goldsby, 2019; Thom et al., 2022). Furthermore, the self-confining nature of the technique allows LTP in olivine to be investigated at room temperature, generating clear microstructural evidence of dislocation activity (Kumamoto et al., 2017; Wallis et al., 2020; Avadanii et al., 2023). These low-temperature experiments are well suited to distinguishing among different models for the influence of water in LTP.

## 2. Methods

Sample M666, a gem-quality single crystal of San Carlos olivine, was hydrated at a pressure of 3 GPa and temperature of 1473 K using a multi-anvil solid-medium apparatus by Li (2015). Fourier transform infrared spectroscopy (FTIR) indicated water concentrations of 1600 ppm H/Si (Li, 2015). To prepare for nanoindentation, one surface of M666 with a surface normal close to [010] was polished using diamond suspensions down to 0.25 μm and finished with 0.05 μm colloidal silica. An initial set of nanoindentation experiments was performed on this water-bearing M666, the results of which are hereafter referred to as M666-W. After performing nanoindentation experiments on M666-W, it was placed in a gas-mixing furnace and held at a temperature of 900°C for 8 hours. A mixture of CO and $CO_2$ was used to maintain the oxygen fugacity at approximately the Ni/NiO buffer and within the stability field of olivine. (At the time dehydration was performed, the furnace temperature was not stable above ~1000°C, so we chose to dehydrate at 900°C for greater control over the oxygen fugacity.) A second set of nanoindentation experiments was performed on this dehydrated M666, the results of which are hereafter referred to as M666-D.

FTIR was performed on M666-D to determine the residual water content, measured to be 700 ppm H/Si in the ~0.4-mm-thick sample (see supplement for methodology). As the value from FTIR is a volume-averaged measurement of water concentration, we used a simple diffusion model to estimate the amount of water that remains in the outer 5 μm of the crystal (see supplement for additional detail). A depth of 5 μm covers the typical region over which olivine deforms during our nanoindentation experiments (~3 times the maximum indent depth), with most strain occurring at even shallower depths (e.g., Avadanii et al., 2023; Wallis et al., 2020). We assume that diffusion along the [010] axis is the relevant dehydration mechanism given the orientation of M666. After 8 hours at 900°C with a diffusion coefficient of $2.05\times10^{-13}$ $m^2s^{-1}$ for

the [010] direction in olivine (Ferriss et al., 2018), our model indicates that the outer 5 μm of the crystal has an average water concentration of 30 ppm H/Si. This value is below the 50 ppm H/Si suggested as the minimum water concentration required for wet creep to be active in olivine (Hirth & Kohlstedt, 2003) and is similar to the water concentration assumed for our dry San Carlos olivine samples (Table 1) based on previous analyses of hydrogen in San Carlos olivine (Denis et al., 2018; Ferriss et al., 2018; Mackwell et al., 1985).

All other samples used in this study (Table S1) were prepared by cutting slices of untreated San Carlos olivine with two parallel sides, then polishing one side using diamond suspensions and colloidal silica, as with M666. Samples were mounted on aluminum stubs with their polished surfaces facing up in preparation for nanoindentation experiments. Crystal orientations were measured using electron backscatter diffraction to ensure that a range of orientations were analyzed (see supplement for more information).

Room-temperature nanoindentation experiments were performed using a MTS Nanoindenter XP and a KLA Nano G200, both equipped with a Berkovich (triangular pyramid) diamond tip. With Berkovich indents, the sharpness of the tip forces the sample to accommodate plastic strain nearly as soon as the indenter tip contacts the sample. In addition, the self-similar shape of the Berkovich tip means that the average magnitude of strain induced by the tip is constant, but the size of the plastic zone increases as the tip is pushed further into the sample over the course of the experiment (e.g., Fischer-Cripps, 2011 p. 7). An example array of 16 indents is shown in Figure 2.

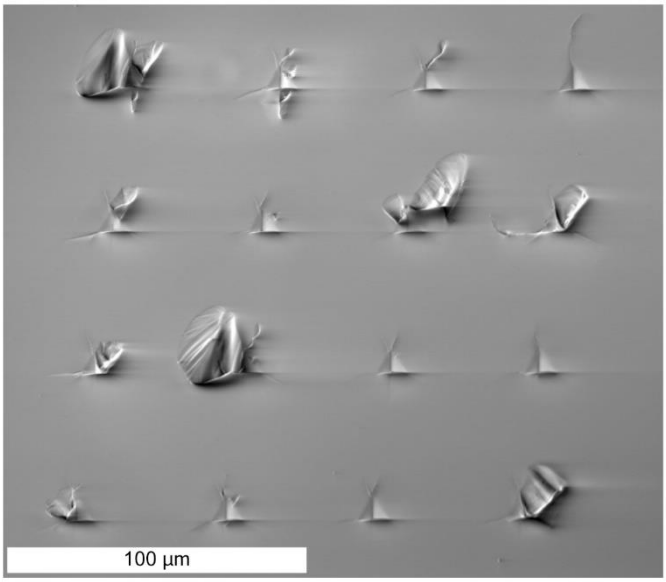


**Figure 2**: A secondary electron image of an array of 16 indents in sample MN1.

Indents were performed using the continuous stiffness method while keeping the ratio of loading rate to load constant at 0.05 $s^{-1}$. The maximum depth of each indent was in the range of 1250–1500 nm for indents on dry olivine and 80–1500 nm for indents on M666-W. A subset of indents on M666-W were performed at different ratios of loading rate to load, from 0.005 $s^{-1}$ to 0.1 $s^{-1}$. Raw data of load on the sample, displacement of the tip into the sample, contact stiffness, and time were recorded for each experiment at a rate of 5 Hz. Data were processed to extract Young's modulus ($E$), hardness ($H$), and yield stress ($\sigma_y$), following the methods by Oliver and Pharr (2004) and Evans and Goetze (1979) and using an area function based on indents performed in fused silica. As the area function is less precise at small indent depths, we only analyze hardness and yield stress for indents deeper than 200 nm. Further details regarding data processing are described in the supplemental information.

## 3. Results

Results are summarized in Table 1 and Figure 3. The elastic behavior of both wet and dry olivine compares very well to previous work (Figure 3B). The moduli for M666-W and M666-D are among the lowest of the tested samples, consistent with their orientation and previous measurements of the elastic properties of olivine (e.g., Zha et al., 1996; Abramson et al., 1997). M666-W exhibits a slightly lower Young's modulus than M666-D, which is expected based on a

previous experimental investigation of the effect of water on the elasticity of olivine (Jacobsen et al., 2008). As observed in previous experiments (Kumamoto et al., 2017), measurements of Young's modulus using nanoindentation exhibit a reduced degree of anisotropy relative to other measurement techniques due to the multiaxial forces applied during nanoindentation experiments.

**Table 1.** Summary of Results

| Dataset | | $E$ (GPa) | $H$ (GPa) | $\sigma_y$ (GPa) | $N$ | Water (ppm H/Si) |
|---|---|---|---|---|---|---|
| M666-W | | 188 ± 7 | 13.3 ± 0.4 | 8.0 ± 0.6 | 44 | 1600[a] |
| M666-D | All | 202 ± 14 | 13.6 ± 0.7 | 7.9 ± 0.6 | 52 | 30[b] |
| | Similar indent ori[d] | 197 ± 5 | 13.4 ± 0.5 | 7.8 ± 0.5 | 16 | |
| San Carlos | All | --- | 12.9 ± 1.0 | 6.9 ± 1.2 | 215 | 40[c] |
| | Similar crystal ori[e] | 208 ± 6 | 13.3 ± 0.5 | 7.4 ± 0.5 | 58 | |

*Note*: Young's modulus ($E$), hardness ($H$), and yield stress ($\sigma_y$) are averaged over a narrow depth range (arbitrarily chosen to be 995–1005 nm) to remove any variation among different samples due to the indentation size effect. $N$ is the number of indentation tests in each group. Data for the average mechanical behavior of San Carlos olivine are a compilation from this study (Table S1) and Kumamoto et al. (2017) and exclude experiments on M666. 95% confidence intervals are reported for all measurements.

[a] From Li (2015).

[b] This water concentration is for the outer 5 μm of M666-D based on diffusion modeling. The water concentration for the whole crystal measured by FTIR is 700 ppm H/Si.

[c] Average based on measurements of water concentration in San Carlos olivine (9 measurements with a range of 0–64 ppm H/Si) by Mackwell et al. (1985), Denis et al. (2018), and Ferriss et al. (2018). Values from Mackwell et al. (1985) have been multiplied by a factor of 3.5 to match the FTIR calibration of Bell et al. (2003) and secondary ion mass spectrometry values.

[d] Averages where the orientation of the Berkovich tip relative to the surface of M666-D was most similar to the orientation of the Berkovich tip relative to the surface of M666-W.

[e] Averages for crystals with surface planes within 10° of the surface plane of M666. These crystals are CT-SCO1, OP1-2-S, and OP3-3 (Table S1).

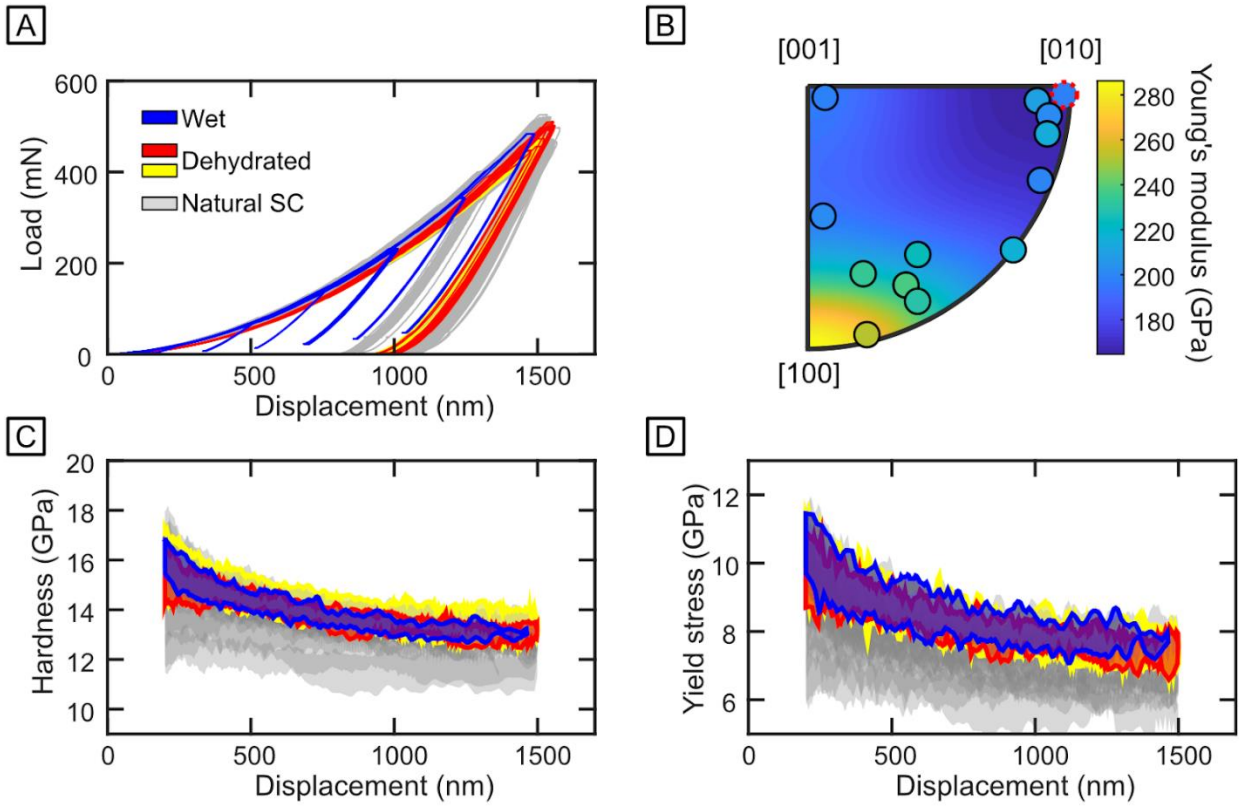


**Figure 3**: Results of 311 Berkovich nanoindentation experiments. (A) Load on the sample versus vertical displacement of the indenter tip into the sample surface. Experiments are shown as individual lines, with experiments on M666-W in blue, M666-D in red, and other dry San Carlos olivine in gray. For the tests on M666-W (blue lines), an artifact associated with how data were exported results in the truncation of the unloading curves but does not affect our results. (B) Average Young's modulus at 1000 nm depth for all samples, plotted at the orientation of the surface normal. M666-D is plotted with a red dashed marker edge. M666-W, which sits at an identical position on the plot, has a slightly lower Young's modulus (Table 1). The background is colored by the uniaxial Young's modulus for dry San Carlos olivine from Abramson et al. (1997). (C) Hardness versus displacement. Results are plotted as envelopes enclosing results at depths greater than 200 nm. Each gray envelope encompasses 7–16 nanoindentation experiments on a single crystal orientation. The blue envelope contains 44 experiments performed on M666-W, and the yellow envelope contains 52 experiments performed on M666-D across 6 different orientations of the indenter tip relative to the sample surface. The red envelope contains a subset of 16 experiments performed on M666-D in the two orientations most similar to the experiments performed on M666-W. (D) Yield stress versus displacement. Envelopes are colored as in (C).

The hardnesses and yield stresses of both wet and dry olivine samples are also consistent with previous measurements. Both quantities vary systematically with orientation (Figure 3C and D). The variability in hardness and yield stress for different crystal orientations at any given indentation depth (~2–3 GPa at depths greater than 500 nm) is approximately the same as that measured previously using spherical nanoindentation (Kumamoto et al., 2017). Due to the complexity of the stress state beneath the indenter tip, many slip systems can be activated

beneath an indent in a crystal of any orientation (e.g., Avadanii et al., 2023; Wallis et al., 2020). The (100)[001] and (110)[001] slip systems are generally the most active at room temperature (e.g., Avadanii et al., 2023; Gaboriaud et al., 1981; Wallis et al., 2020) due to their low critical resolved shear stresses (e.g., Hansen et al., 2019). Thus the observed anisotropy in hardness and yield stress in our results is primarily due to different resolved shear stresses on these slip systems depending on the geometry of deformation under the indenter tip.

The nanoindentation tests exhibit the indentation size effect in that hardness decreases with increasing indent depth (e.g., Nix & Gao, 1998; Pharr et al., 2010; Kumamoto et al., 2017; Koizumi et al., 2020). The size effect for each orientation can be characterized by a power law, with the exponent ranging from -0.03 to -0.17. Yield stress, calculated from modulus and hardness following the method of Evans and Goetze (1979), has a similar relationship with indent size, with a power-law exponent ranging from -0.02 to -0.22. Previous indentation studies on olivine identified size effects of similar magnitudes (Kumamoto et al., 2017; Koizumi et al., 2020).

When directly compared, measurements of hardness and yield stress for M666-W and M666-D overlap for nearly the entire experimental range of depths (Figure 3C and D). Small differences between the datasets on M666-W and M666-D can be attributed to the azimuthal anisotropy of the Berkovich tip. We tested 6 different tip orientations on M666-D by rotating the triangular pyramidal Berkovich tip about its axis of symmetry and then indenting the same crystal surface. We found that at a depth of 1000 nm, the modulus varied by 7%, the hardness varied by 4%, and the yield stress varied by 3% (Table S1). In contrast, the difference between M666-W and M666-D for similar indent orientations (the red fields in Figure 3C and D; “similar indent ori” in Table 1) is 0.6% for hardness and 2% for yield stress. Thus, even the minor anisotropy induced by the orientation of the indenter tip relative to a single crystal surface has a greater effect on hardness and yield stress than that of the water content.

## 4. Discussion

In a previous study on the role of water in glide-controlled deformation of olivine, Katayama and Karato (2008) interpreted the weakening effect of water in their experiments as being due to a reduction in the Peierls stress by a factor of ~3. They suggested this single mechanism could

describe the effect of water on both low- and high-temperature rheological behavior due to the influence of the Peierls stress on the formation energy of both kinks and jogs (local displacements of the dislocation perpendicular to the glide plane). This type of weakening corresponds to model 4 (Figure 1).

Our experiments at low temperature demonstrate that the Peierls stress is not lowered by high water concentrations, ruling out model 4. M666-W and M666-D are extremely similar in hardness and yield stress despite the significant difference in water content (Table 1, Figure 3). Dry olivine samples in similar orientations (e.g., CT-SCO1) are also quite close to M666-W in their mechanical properties (Table 1, Table S1). The difference in yield stress of 0.1–0.2 GPa between M666-W and M666-D is within the 95% confidence interval of ±0.6 GPa on the yield stresses and is an order of magnitude less than the effect of anisotropy due to crystal orientation observed in this study. The similarities in mechanical behavior between M666-D and M666-W suggest that any effect of water on dislocation glide is inconsequential at room temperature. By comparison, in the dislocation-creep regime at a temperature of 1250°C and a constant strain rate of $10^{-5}$ $s^{-1}$, we would expect the strength of M666-W to be ~30% of that of dry olivine (see supplemental material for specific flow-law parameters).

Other models presented for hydrolytic weakening in olivine (Figure 1) are still possible. For instance, the Peierls stress could still be reduced at elevated temperatures (model 3). $H^+$ may also lead to weakening at high temperatures and not at low temperatures by increasing the kink concentration (model 2) or increasing diffusivities and reducing the backstress (model 1).

Our results demonstrate that intracrystalline $H^+$ has little to no impact on olivine deformation at low temperatures. For instance, intracrystalline water likely does not affect the frictional strength of faults if frictional strength is controlled by dislocation motion near contacts between plastically deforming asperities (e.g., Aharonov & Scholz, 2019; Boettcher et al., 2007; Tabor, 1981; Thom et al., 2022). Intracrystalline water also likely does not influence the maximum strength of the lithosphere near the brittle-ductile transition, at which LTP acts in tandem with brittle deformation mechanisms (e.g., Warren & Hansen, 2023).

**Acknowledgements**

The authors would like to thank Jed Mosenfelder for performing FTIR analyses, David Kohlstedt for analyzing the FTIR data, Kay Song for performing EBSD analyses, Christopher Thom for useful discussions regarding nanoindentation, and reviewer Jacob Tielke and editor Quentin Williams for their thoughtful comments. Funding for this project was provided by National Science Foundation grants EAR-1255620 and EAR-1625032 to JMW, EAR-1806791 to KMK, and EAR-2022433 to LNH, Natural Environment Research Council grant NE/M000966/1 to LNH, the Netherlands Organisation for Scientific Research, User Support Programme Space Research, grant ALWGO.2018.038 to DW and LNH and grant ENW.GO.001.005 to DW, TB and LNH, UKRI Future Leaders Fellowship grant MR/V021788/1 to DW, and a fellowship from the Royal Commission for the Exhibition of 1851 to TB. This work was partially performed under the auspices of the U.S. Department of Energy by Lawrence Livermore National Laboratory under Contract DE-AC52-07NA27344. LLNL-JRNL-853683

**Open Research: Data Availability Statement**

Berkovich nanoindentation and FTIR data gathered for this study are available at Kumamoto et al. (2023).

# References


Abramson, E. H., Brown, J. M., Slutsky, L. J., & Zaug, J. (1997). The elastic constants of San Carlos olivine to 17 GPa. *Journal of Geophysical Research*, *102*(B6), 12253–12263.

Aharonov, E., & Scholz, C. H. (2019). The Brittle-Ductile Transition Predicted by a Physics-based Friction Law. *Journal of Geophysical Research: Solid Earth, 123*(3), 2721-2737. https://doi.org/10.1029/2018JB016878

Avadanii, D., Hansen, L., Marquardt, K., Wallis, D., Ohl, M., & Wilkinson, A. (2023). The role of grain boundaries in low-temperature plasticity of olivine revealed by nanoindentation. *Journal of Geophysical Research: Solid Earth, 128*(8), e2023JB026763. https://doi.org/10.1029/2023jb026763

Bai, Q., & Kohlstedt, D. L. (1992). High-temperature creep of olivine single crystals, 2. dislocation structures. *Tectonophysics*, *206*(1), 1–29. https://doi.org/10.1016/0040-1951(92)90365-D

Bell, D. R., & Rossman, G. R. (1992). Water in Earth's Mantle: The Role of Nominally Anhydrous Minerals. *Science*, *255*(5050), 1391–1397. https://doi.org/10.1126/science.255.5050.1391

Bell, D. R., Rossman, G. R., Maldener, J., Endisch, D., & Rauch, F. (2003). Hydroxide in olivine: A quantitative determination of the absolute amount and calibration of the IR spectrum. *Journal of Geophysical Research*, *108*(B2), 672. https://doi.org/10.1029/2001JB000679

Boettcher, M. S., Hirth, G., & Evans, B. (2007). Olivine friction at the base of oceanic seismogenic zones. *Journal of Geophysical Research: Solid Earth, 112*, B01205. https://doi.org/10.1029/2006jb004301

Breithaupt, T., Katz, R. F., Hansen, L. N., & Kumamoto, K. M. (2023). Dislocation theory of steady and transient creep of crystalline solids: Predictions for olivine. *Proceedings of the National Academy of Sciences*, *120*(8), e2203448120. https://doi.org/10.1073/pnas.2203448120

Buffett, B. A., & Becker, T. W. (2012). Bending stress and dissipation in subducted lithosphere. *Journal of Geophysical Research: Solid Earth, 117*, B05413. https://doi.org/10.1029/2012jb009205

Bunge, H. (1982). *Texture Analysis in Materials Science: Mathematical Methods*. London: Butterworth and Co.

Denis, C. M. M., Demouchy, S., & Alard, O. (2018). Heterogeneous hydrogen distribution in orthopyroxene from veined mantle peridotite (San Carlos, Arizona): Impact of melt-rock interactions. *Lithos*, *302-303*, 298–311. https://doi.org/10.1016/j.lithos.2018.01.007

Dixon, N. A., & Durham, W. B. (2018). Measurement of Activation Volume for Creep of Dry Olivine at Upper-Mantle Conditions. *Journal of Geophysical Research: Solid Earth*, *123*(10), 8459–8473. https://doi.org/10.1029/2018JB015853

Evans, B., & Goetze, C. (1979). The temperature variation of hardness of olivine and its implication for polycrystalline yield stress. *Journal of Geophysical Research*, *84*(B10), 5505. https://doi.org/10.1029/JB084iB10p05505

Ferriss, E., Plank, T., Newcombe, M., Walker, D., & Hauri, E. (2018). Rates of dehydration of olivines from San Carlos and Kilauea Iki. *Geochimica et Cosmochimica Acta*, *242*, 165–190. https://doi.org/10.1016/j.gca.2018.08.050

Fischer-Cripps, A. C. (2011). *Nanoindentation*. New York, NY: Springer Science+Business Media, LLC.

Gaboriaud, R. J., Darot, M., Gueguen, Y., & Woirgard, J. (1981). Dislocations in olivine indented at low temperatures. *Physics and Chemistry of Minerals*, *7*(2), 100–104. https://doi.org/10.1007/BF00309460

Griggs, D. (1967). Hydrolytic Weakening of Quartz and Other Silicates. *Geophysical Journal International*, *14*(1-4), 19–31. https://doi.org/10.1111/j.1365-246X.1967.tb06218.x

Griggs, D. (1974). A model of hydrolytic weakening in quartz. *Journal of Geophysical Research*, *79*(11), 1653–1661. https://doi.org/10.1029/JB079i011p01653

Hansen, L. N., Kumamoto, K. M., Thom, C. A., Wallis, D., Durham, W. B., Goldsby, D. L., et al. (2019). Low-temperature plasticity in olivine: Grain size, strain hardening, and the strength of the lithosphere. *Journal of Geophysical Research: Solid Earth*, *124*, 5427–5449. https://doi.org/10.1029/2018JB016736

Hansen, L. N., Wallis, D., Breithaupt, T., Thom, C. A., & Kempton, I. (2021). Dislocation creep of olivine: Backstress evolution controls transient creep at high temperatures. *Journal of Geophysical Research, [Solid Earth]*, *126*(5). https://doi.org/10.1029/2020jb021325

Heggie, M., & Jones, R. (1986). Models of hydrolytic weakening in quartz. *Philosophical Magazine A*, *53*(5), L65–L70. https://doi.org/10.1080/01418618608242857

Hirth, G., & Kohlstedt, D. L. (2003). Rheology of the upper mantle and the mantle wedge: A view from the experimentalists. In J. Eiler (Ed.), *Inside the Subduction Factory, Geophysical Monograph Series* (Vol. 138, pp. 83–105). Washington, DC: American Geophysical Union.

Hobbs, B. E. (1984). Point defect chemistry of minerals under a hydrothermal environment. *Journal of Geophysical Research*, *89*(B6), 4026–4038. https://doi.org/10.1029/JB089iB06p04026

Ingrin, J., & Blanchard, M. (2006). Diffusion of Hydrogen in Minerals. *Reviews in Mineralogy and Geochemistry*, *62*(1), 291–320. https://doi.org/10.2138/rmg.2006.62.13

Jacobsen, S. D., Jiang, F., Mao, Z., Duffy, T. S., Smyth, J. R., Holl, C. M., & Frost, D. J. (2008). Effects of hydration on the elastic properties of olivine. *Geophysical Research Letters*, *35*(14), 2105. https://doi.org/10.1029/2008GL034398

Kalidindi, S. R., & Vachhani, S. J. (2014). Mechanical characterization of grain boundaries using nanoindentation. *Current Opinion in Solid State and Materials Science*, *18*(4), 196–204. https://doi.org/10.1016/j.cossms.2014.05.002

Karato, S.-I. (2008). *Deformation of Earth Materials: An Introduction to the Rheology of Solid Earth*. Cambridge University Press.

Katayama, I., & Karato, S.-I. (2008). Low-temperature, high-stress deformation of olivine under water-saturated conditions. *Physics of the Earth and Planetary Interiors*, *168*(3), 125–133. https://doi.org/10.1016/j.pepi.2008.05.019

Keefner, J. W., Mackwell, S. J., Kohlstedt, D. L., & Heidelbach, F. (2011). Dependence of dislocation creep of dunite on oxygen fugacity: Implications for viscosity variations in Earth's mantle. *Journal of Geophysical Research*, *116*, B05201. https://doi.org/10.1029/2010JB007748

Kohlstedt, D. L. (2006). The Role of Water in High-Temperature Rock Deformation. *Reviews in Mineralogy and Geochemistry*, *62*(1), 377–396. https://doi.org/10.2138/rmg.2006.62.16

Koizumi, S., Hiraga, T., & Suzuki, T. S. (2020). Vickers indentation tests on olivine: size effects. *Physics and Chemistry of Minerals*, *47*(2), 8. https://doi.org/10.1007/s00269-019-01075-5

Kranjc, K., Rouse, Z., Flores, K. M., & Skemer, P. (2016). Low-temperature plastic rheology of olivine determined by nanoindentation. *Geophysical Research Letters*, *43*(1), 176–184. https://doi.org/10.1002/2015GL065837

Kumamoto, K. M., Thom, C. A., Wallis, D., Hansen, L. N., Armstrong, D. E. J., Warren, J. M., et al. (2017). Size effects resolve discrepancies in 40 years of work on low-temperature plasticity in olivine. *Science Advances*, *3*(9), e1701338. https://doi.org/10.1126/sciadv.1701338

Kumamoto, K.M., Breithaupt, T.P., Hansen, L.N., Wallis, D., Li, B.-S., Armstrong, D.E.J., Goldsby, D.L., Li, Y., Warren, J.M., & Wilkinson, A.J. (2023) Berkovich nanoindentation and FTIR data describing the effect of water on olivine. Retrieved from the Data Repository for the University of Minnesota, https://hdl.handle.net/11299/256166

Li, Y. (2015). *Hydrogen incorporation mechanisms and diffusion of hydrous defects and silicon ions in olivine: the major rock-forming mineral of the Earth's upper mantle* (Ph.D.). Retrieved from University of Minnesota Libraries (http://hdl.handle.net/11299/177141). Location: University of Minnesota

Lynn, K. J., & Warren, J. M. (2021). The potential for aqueous fluid-rock and silicate melt-rock interactions to re-equilibrate hydrogen in peridotite nominally anhydrous minerals. *The American Mineralogist*, *106*(5), 701–714. https://doi.org/10.2138/am-2021-7435

Mackwell, S. J., Kohlstedt, D. L., & Paterson, M. S. (1985). The role of water in the deformation of olivine single crystals. *Journal of Geophysical Research*, *90*(B13), 11319-11333. https://doi.org/10.1029/JB090iB13p11319

Nix, W. D., & Gao, H. (1998). Indentation size effects in crystalline materials: A law for strain gradient plasticity. *Journal of the Mechanics and Physics of Solids*, *46*(3), 411–425. https://doi.org/10.1016/S0022-5096(97)00086-0

Oliver, W. C., & Pharr, G. M. (1992). An improved technique for determining hardness and elastic modulus using load and displacement sensing indentation experiments. *Journal of Materials Research*, *7*(6), 1564–1583. https://doi.org/10.1557/JMR.1992.1564

Oliver, W. C., & Pharr, G. M. (2004). Measurement of hardness and elastic modulus by instrumented indentation: Advances in understanding and refinements to methodology. *Journal of Materials Research*, *19*(1), 3–20. https://doi.org/10.1557/jmr.2004.19.1.3

Paterson, M. S. (1982). The determination of hydroxyl by infrared adsorption in quartz, silicate glasses and similar materials. *Bulletin de Mineralogie*, *105*, 20–29.

Pharr, G. M., Herbert, E. G., & Gao, Y. (2010). The Indentation Size Effect: A Critical Examination of Experimental Observations and Mechanistic Interpretations. *Annual Review of Materials Research*, *40*(1), 271–292. https://doi.org/10.1146/annurev-matsci-070909-104456

Tabor, D. (1981). Friction—The Present State of Our Understanding. *Journal of Lubrication Technology*, *103*(2), 169–179. https://doi.org/10.1115/1.3251622

Thom, C. A., & Goldsby, D. L. (2019). Nanoindentation Studies of Plasticity and Dislocation Creep in Halite. *Geosciences Journal*, *9*(2), 79. https://doi.org/10.3390/geosciences9020079

Thom, C. A., Hansen, L. N., Breithaupt, T., Goldsby, D. L., & Kumamoto, K. M. (2022). Backstresses in geologic materials quantified by nanoindentation load-drop experiments. *Philosophical Magazine*, *102*(19), 1974–1988. https://doi.org/10.1080/14786435.2022.2100937

Tielke, J. A., Zimmerman, M. E., & Kohlstedt, D. L. (2017). Hydrolytic weakening in olivine single crystals. *Journal of Geophysical Research: Solid Earth*, *122*(5), 3465–3479. https://doi.org/10.1002/2017JB014004

Wallis, D., Hansen, L. N., Kumamoto, K. M., Thom, C. A., Plümper, O., Ohl, M., et al. (2020). Dislocation interactions during low-temperature plasticity of olivine and their impact on the evolution of lithospheric strength. *Earth and Planetary Science Letters*, *543*, 116349. https://doi.org/10.1016/j.epsl.2020.116349

Wang, D., Mookherjee, M., Xu, Y., & Karato, S.-I. (2006). The effect of water on the electrical conductivity of olivine. *Nature*, *443*(7114), 977–980. https://doi.org/10.1038/nature05256

Warren, J. M., & Hansen, L. N. (2023). Ductile Deformation of the Lithospheric Mantle. *Annual Review of Earth and Planetary*. https://doi.org/10.1146/annurev-earth-031621-063756

Zha, C.-S., Duffy, T. S., Downs, R. T., Mao, H.-K., & Hemley, R. J. (1996). Sound velocity and elasticity of single-crystal forsterite to 16 GPa. *Journal of Geophysical Research*, *101*(B8), 17535–17545. https://doi.org/10.1029/96JB01266